Three-body correlations in the variational wave function of liquid ^{4}He

V. R. Pandharipande
Department of Physics, University of Illinois at Urbana-Champaign, Urbana, Illinois 61801
(Received 27 December 1977)

A product of two-body (f_{ij}) and three-body (f_{ijk}) correlation functions is used as a variational wave function for liquid ^{4}He. The f_{ijk} take into account the backflows produced by two particles recoiling from each other. The distribution functions, the energy, and its uncertainty are all calculated using the Lennard-Jones-deBoer-Michel potential, and diagrammatic hypernetted-chain summation methods. The calculated equilibrium energy of -6.72 (± 0.2)°K, is significantly lower than the -5.9°K obtained with only a product of f_{ij}, and agrees with the -6.84°K estimated from a Monte Carlo integration of the many-body Schrödinger equation. The proposed wave function is simple enough to be useful in Fermi liquids.

I. INTRODUCTION

An upper bound to the energy of Bose liquids may be easily calculated[1] with the "Jastrow" wave function

$$\psi_J = \prod_{i<j} f_{ij}, \tag{1.1}$$

using a single-parameter set of correlation functions, obtained by minimizing the two-body cluster contribution with constraint $f(r>d)=1$. The energy can be accurately calculated for this class of f's with the hierarchy of hypernetted chain equations and minimized with respect to variations in the "healing distance" d. The approximations in this method are discussed in Ref. 1, and they have little influence on the energies calculated within the functional space spanned by (1.1).

In the present work the method of constrained variation is further developed to obtain a two-parameter set of variational wave type:

$$\psi_v = \prod_{i<j} f_{ij} \prod_{i<j<k} f_{ijk}. \tag{1.2}$$

The three-body correlation f_{ijk} primarily takes into account the Feynman-Cohen[2] backflows produced by two-particles recoiling from each other in the liquid.

The calculation of the two-parameter wave function (1.2) is discussed in Sec. II, while Sec. III illustrates the use of standard cluster-expansion and chain-summation techniques to calculate distribution functions and expectation values. A set of coupled-integral equations which sums hypernetted chains of a selected class is used to calculate the ground-state energy and density of liquid ^{4}He in Sec. IV. The equilibrium E_0 and ρ_0 calculated using the Lennard-Jones–deBoer-Michels potential are, respectively, -6.72 °K and $1.04\rho_e$; as against -5.9 °K and $0.9\rho_e$ obtained in the "Jastrow" approximation, and -7.14 °K and ρ_e from experiment.

Several diagrams neglected in the above calculation are studied in Sec. V to estimate the accuracy of the calculation to be ≈0.2 °K. This estimate includes the effect of the neglected long-range pair correlations as well as that of the three-body triple dipole interaction.[3] At least two other methods have been used to improve upon the "Jastrow" wave function. These are Feenberg's perturbation theory in the correlated basis,[4] and the "Green's-function" Monte Carlo method.[5] A comparison of the results obtained with these methods is given in Sec. VI.

II. THE VARIATIONAL WAVE FUNCTION

In the context of Fermi fluids Pandharipande and Bethe[6] studied the correlated wave function $\psi(\vec{k},\vec{r})$ of a pair of particles with a relative momentum $\vec{k}$ by constrained variation. The $\psi(\vec{k},\vec{r})$ is conveniently expressed as

$$\psi(\vec{k},\vec{r}) = \sum_{l=0}^{\infty} i^l (2l+1) f(l,k,r) j_l(kr) P_l(\cos\theta), \tag{2.1}$$

and the correlation function $f(l,k,r)$ in the lth partial wave is obtained from the equations

$$u_l(k,r) = f(l,k,r) j_l(kr) r, \tag{2.2}$$

$$-\frac{\hbar^2}{m}\left(u_l''(k,r) - \frac{l(l+1)}{r^2}u_l(k,r)\right) + v u_l(k,r) = \left(\frac{\hbar^2}{m}k^2 + \lambda_l(k)\right) u_l(k,r). \tag{2.3}$$

The "Schrödinger" Eq. (2.3) is valid for $r<d$, and $\lambda_l(k)$ is obtained from the boundary condition $f'(l,k,r=d)=0$.

We may now define a complex correlation function $f(\vec{k},\vec{r})$ such that

$$f(\vec{k},\vec{r})\, e^{i\vec{k}\cdot\vec{r}} = \psi(\vec{k},\vec{r}). \tag{2.4}$$

In the limit $k \to 0$ the $f(\vec{k}, \vec{r})$ reduces to a simple operator $\mathcal{F}$, (Ref. 7),

$$\mathcal{F} = f(l=0, k\to 0, r) + [f(l=1, k\to 0, r) - f(l=0, k\to 0, r)]\hat{r}\cdot\nabla \equiv f + \eta\vec{r}\cdot\nabla . \tag{2.5}$$

The second term of $\mathcal{F}$ generates the Feynman-Cohen backflow and successfully explains the effective mass of ^{3}He impurities in liquid ^{4}He.[7] Even though the above $\mathcal{F}$ is strictly valid only at small $|k|$ it certainly is better than f by itself. As a matter of fact, the contribution of the $\eta\vec{r}\cdot\nabla$ term to the two-body cluster energy

$$\int d^3r\, e^{-i\vec{k}\cdot\vec{r}}\mathcal{F}^\dagger\left(-\frac{\hbar^2}{m}(\nabla^2+k^2)+v\right)\mathcal{F}\, e^{i\vec{k}\cdot\vec{r}} - \int d^3r\, e^{-i\vec{k}\cdot\vec{r}} f\left(-\frac{\hbar^2}{m}(\nabla^2+k^2)+v\right) f\, e^{i\vec{k}\cdot\vec{r}} = \frac{4\pi}{3}k^2\int \eta\left(-\frac{\hbar^2}{m}[(f'+\eta')4r+\eta'' r^2]+v\eta\right) r^2\, dr , \tag{2.6}$$

is proportional to k^2 at all values of k.

The operators $\mathcal{F}_{ij}, \mathcal{F}_{ik}, \ldots$ do not commute, and thus the variational wave function has to be defined as

$$\Psi = S\prod_{i<j}[f_{ij} + \tfrac{1}{2}\eta_{ij}\vec{r}_{ij}\cdot(\vec{\nabla}_i - \vec{\nabla}_j)] , \tag{2.7}$$

where S is a symmetrizing operator. This wave function is a bit complicated, though it may be possible to work with it using the cluster expansion developed by Wiringa and Pandharipande[8] for noncommuting correlation operators.

The η_{ij} is quite small ($\approx$0.2 at the maximum) and we may expand (2.7) in powers of η. The zeroth order corresponds to the single-parameter Jastrow wave function

$$\Psi_J(d) = \prod_{i<j} f_{ij}(d) \tag{2.8}$$

used in Ref. 1. As a next approximation we consider

$$\Psi_v(d) = \prod_{i<j} f_{ij} \prod_{i<j<k}\left[1 + \sum_{\text{cyc}} \frac{1}{4}\left(\frac{\eta_{ij}\vec{r}_{ij}\cdot(\vec{\nabla}_i f_{ik})}{f_{ij}f_{ik}} + \frac{\eta_{ik}\vec{r}_{ik}\cdot(\vec{\nabla}_i f_{ij})}{f_{ik}f_{ij}}\right)\right], \tag{2.9}$$

which has the desired form (1.2) and is correct up to terms linear in η. $\sum_{\text{cyc}}$ represents a sum of the three terms obtained by replacing ijk by jki and kij. Finally, we note that η and f'_{ij} are both sharply peaked beyond the core, and have similar shapes. Thus, instead of (2.9), we may use the simpler wave function

$$\Psi_v(d,\beta) = \prod_{i<j} f_{ij}(d) \prod_{i<j<k}\left(1 + \sum_{\text{cyc}} \xi_{ij}(d,\beta) \times \xi_{ik}(d,\beta)\vec{r}_{ij}\cdot\vec{r}_{ik}\right) \equiv \prod_{i<j} f_{ij} \prod_{i<j<k}\left(1 + \sum_{\text{cyc}} \chi_{ijk}\right), \tag{2.10}$$

$$\xi(d,\beta) = \beta\frac{\eta(d)}{f(d)} , \tag{2.11}$$

and treat β as an additional variational parameter. At equilibrium β should be of order of the square root of the average value of $f'/2\eta r$.

III. CLUSTER EXPANSION AND CHAIN SUMMATION

A diagrammatic cluster expansion of the expectation value of an operator $O_{mn}(r_{mn})$

$$\frac{\int \prod_{i<j} f_{ij} \prod_{i<j<k}(1+\sum_{\text{cyc}}\chi_{ijk})\, O_{mn}(r_{mn}) \prod_{i<j<k}(1+\sum_{\text{cyc}}\chi_{ijk}) \prod_{i<j} f_{ij}\, d\tau}{\int \prod_{i<j} f_{ij}^2 \prod_{i<j<k}(1+\sum_{\text{cyc}}\chi_{ijk})^2\, d\tau} \tag{3.1}$$

is obtained by replacing all the f^2 except f_{mn}^2 in the numerator by $1+F$. (This F should not be confused with the $\mathcal{F}$ operator in Sec. II.) The integrals in the numerator and the denominator are then represented by diagrams in which the points represent the particle coordinates, a wiggly line joining m and n represents the function $f_{mn}O_{mn}f_{mn}$, F_{ij} is a dashed line ij, and solid lines ij and ik with a marking on the angle i of the triangle ijk denote χ_{ijk}. The numerator diagrams must contain the wiggly line mn, and the expectation value is given by the sum of all irreducible numerator diagrams. Similarly the expectation value of a three-body operator O_{mn0} is given by the sum of all irreducible diagrams containing a triangle $mn0$ representing

$$f_{mn}f_{m0}f_{n0}\left(1+\sum_{\text{cyc}}\chi_{mn0}\right) O_{mn0}\left(1+\sum_{\text{cyc}}\chi_{mn0}\right) f_{mn}f_{m0}f_{n0} . \tag{3.2}$$

In the hypernetted chain (HNC) approximation all diagrams containing single or multiple chains connecting two particles are summed, neglecting the coupling between the chains. The validity of the HNC approximation may be ascertained by an HNC/4 calculation[1] in which the effect of pairwise coupling between the hypernetted chains is

calculated. The following are integral-equations sum-hypernetted chains formed from the F_{ij} and χ_{ijk}:

$$C_{1,mn}=\rho\int (g-1-C_1)_{m1}(g-1)_{n1}\,d^3r_1\,,$$

$$C_{2,mn}=\rho\int (\tilde{g}\xi r)_{m1}(\tilde{g}\xi r)_{n1}\cos\theta_1\,d^3r_1\,,$$

$$C_{3,mn}=\rho(\xi r)_{mn}\int (\tilde{g}\xi r)_{m1}\tilde{g}_{n1}\cos\theta_m\,d^3r_1\,,$$

$$C_{4,mn}=\rho\int (\tilde{g}\xi^2r^2)_{m1}(\tilde{g}\xi^2r^2)_{n1}\cos^2\theta_1\,d^3r_1\,,$$

$$C_{5,mn}=\rho(\xi^2r^2)_{mn}\int (\tilde{g}\xi^2r^2)_{m1}\tilde{g}_{n1}\cos^2\theta_m\,d^3r_1\,, \tag{3.3}$$

$$C_{6,mn}=\rho(\xi r)_{mn}\int (\tilde{g}\xi^2r^2)_{m1}(\tilde{g}\xi r)_{n1}\cos\theta_m\cos\theta_1\,d^3r_1\,,$$

$$C_{7,mn}=\rho(\xi^2r^2)_{mn}\int (\tilde{g}\xi r)_{m1}(\tilde{g}\xi r)_{n1}\cos\theta_m\cos\theta_n\,d^3r_1\,,$$

$$\tilde{g}=f^2\exp(C_1)\,,$$

$$g=\tilde{g}(1+2C_2+4C_3+C_4+2C_5+4C_6+2C_7)\,.$$

Figure 1 shows some of the simpler chains summed by C_1 [diagrams (1.1)–(1.3)], and $C_{2\text{-}7}$ [diagrams (1.4)–(1.9)].

The C_2 diagrams can have the χ_{1mn} from either Ψ or Ψ^*, and thus their contribution to the two-particle distribution function g is $2\tilde{g}C_2$. The C_3 diagrams may be formed from χ_{m1n} or χ_{n1m} from Ψ or Ψ^* and thus get multiplied by four in the g equation. The $C_{4\text{-}7}$ take care of the nine terms in the product of $\sum_{\text{cyc}}\chi_{mn1}$ in Ψ^* with $\sum_{\text{cyc}}\chi_{mn1}$ in Ψ. We note that the above equations do not sum diagrams having more than one χ involving a pair of particles such as χ_{ijk}, χ_{iji}. These are discussed in Sec. V.

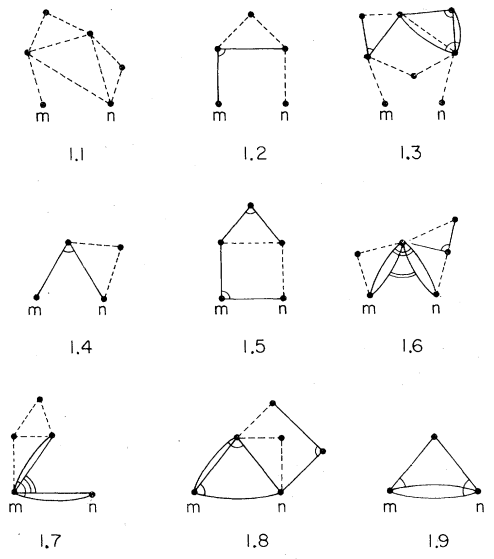

FIG. 1. Some of the simpler chain diagrams summed by Eq. (3.3) for C_1–C_7.

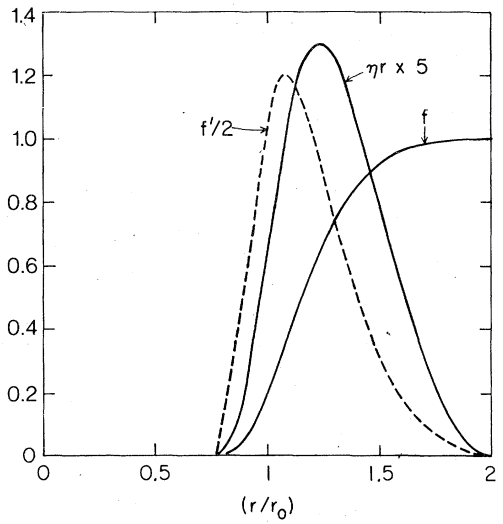

FIG. 2. f, ηr, and f' in ^{4}He at ρ_e, $d=2r_0$.

Figures 2–4 show some of the functions calculated at ρ_e, $d=2r_0$, and $\beta=1.65$. The above values for the parameters are quite close to the equilibrium. The f' is reasonably similar to ηr

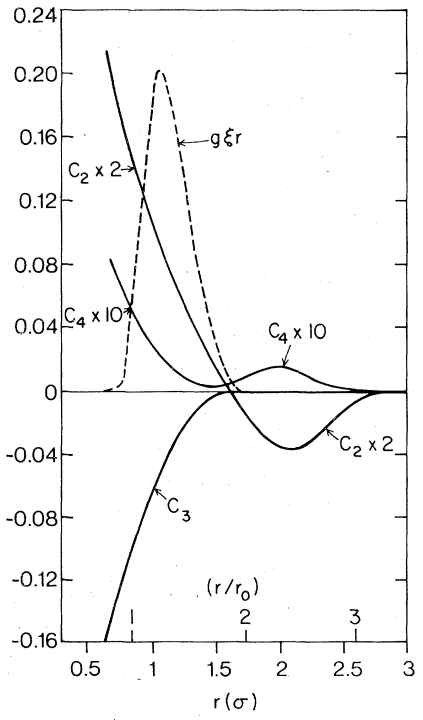

FIG. 3. $g\xi r$ and C_2–C_4 in ^{4}He at ρ_e, $d=2r_0$, $\beta=1.65$.

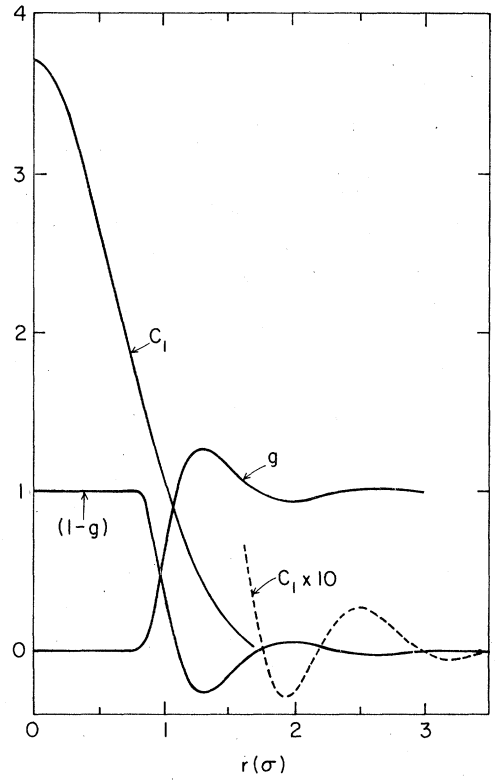

FIG. 4. g, $(1-g)$, and C_1, in ^{4}He at ρ_e, $d=2r_0$, $\beta=1.65$.

(Fig. 2), and hence the approximation of the wave function (2.9) by (2.10) may not be bad.

The $g\xi r$ [Fig. (3)] is a function peaked around 1.1σ; the Lennard-Jones potential changes sign at $r=\sigma=2.556$ Å. Thus C_2, which has a $\cos\theta_1$ in its integrand changes sign at $r_{mn}\sim\sqrt{2}\times1.1\sigma$. The angle $m1n$ is $\approx\frac{1}{2}\pi$ for $r_{m1}\approx r_{n1}\approx1.1\sigma$, and $r_{mn}\sim\sqrt{2}\times1.1\sigma$. The C_3 is negative and goes to zero at $r=d$. Due to the $\cos^2\theta_1$ in its integrand, C_4 has a minimum at $\approx\sqrt{2}\times1.1\sigma$. It is second order in χ and thus rather small in magnitude. The $C_{5,6,7}$ (not shown in Fig. 3) are all positive and have a range d. Inside d they are comparable to C_4 in magnitude.

The C_1 (Fig. 4) oscillates at large r and becomes large positive at $r<1.5\sigma$. It is larger than $C_{2\text{-}7}$ by an order of magnitude; and it is also bigger than $(1-g)$. There is no prominent influence of χ_{ijk} on the $g(r)$, it merely increases the structure by a small amount. At its first maximum and minimum the $g(r)$ for ρ_e, $d=2r_0$, and $\beta=0$ (no χ) is 1.254 and 0.953 in the HNC approximation, while for $\beta=1.65$ it is 1.266 and 0.942, respectively.

Two technical points may be mentioned here: First, the f and η are practically zero for $r<0.5\sigma$, while ξ diverges as $1/r$ at small r. This divergence has no practical significance since ξ is always multiplied by r and f, however to avoid numerical problems we set ξ to zero at $r\lesssim0.5\sigma$ where $g(r)$ becomes less than 10^{-10}. Second, the required combination of C_2–C_7 in the Eq. (3.3) for g may be directly computed in a single integral as follows:

$$(2C_2+4C_3+C_4+2C_5+4C_6+2C_7)_{mn}=\rho\int\left[\left(1+\sum_{\text{cyc}}\chi_{mn1}\right)^2-1\right]\tilde{g}_{m1}\tilde{g}_{n1}\,d^3r_1. \quad (3.4)$$

IV. THE CALCULATION OF ENERGY

The contribution to the energy expectation value of terms containing the two-body potential v_{mn} and a part of the kinetic energy coming from $-(\hbar^2/2m)(\nabla_m^2 f_{mn})$ is called W,[1] and is given by

$$W=\frac{\rho\lambda_0(k\to0)}{2}\int_0^d 4\pi r^2 g(r)\,dr+\frac{\rho}{2}\int_d^\infty 4\pi r^2 v(r)g(r)\,dr. \quad (4.1)$$

This contribution is very insensitive to the three-body correlation χ as can be seen from Table I.

The fraction of kinetic energy due to $-(\hbar^2/m)\vec{\nabla}_m f_{mn}\cdot\vec{\nabla}_m f_{m0}$ is called U (Ref. 1);

$$U=-\frac{\hbar^2}{2m}\rho^2\int\tilde{g}_{mn}\tilde{g}_{m0}\tilde{g}_{n0}\left(1+\sum_{\text{cyc}}\chi_{mn0}\right)^2\frac{f'_{mn}f'_{m0}}{f_{mn}f_{m0}}\times\cos\theta_m\,d^3r_{mn}\,d^3r_{m0}, \quad (4.2)$$

and it decreases rapidly with β (Table II). The term linear in χ_{mn0} causes most of the reduction; it has a $\cos^2\theta_m$ in the integrand and is negative definite.

Figure 5 illustrates the various terms of type $(\nabla_m^2\sum_{\text{cyc}}\chi_{mn0})$ and $(\vec{\nabla}_m f_{mn})\cdot(\vec{\nabla}_m\sum_{\text{cyc}}\chi_{mn0})$ that contribute to the kinetic energy. The filled, hollow, and open arrows along line ij, respectively, represent the ∇_i of f_{ij}, $\vec{r}_{ij}$, and ξ_{ij}, while a double open

TABLE I. Composition of $E(\rho_e,\ d=2r_0,\ \beta)$.

β	0	1.45	1.65	1.85
W	-10.011	-10.013	-10.014	-10.015
U	+ 4.362	+ 2.550	+ 1.941	+ 1.233
T	0	+ 0.871	+ 1.394	+ 2.133
E	- 5.649	- 6.592	- 6.679	- 6.649

TABLE II. $E(\rho_e,\ d,\ \beta_{\min})$.

d/r_0	$\beta_{\min}$	$E(d,\beta_{\min})$
1.8	2.5	-6.643
2.0	1.7	-6.679
2.2	1.35	-6.504

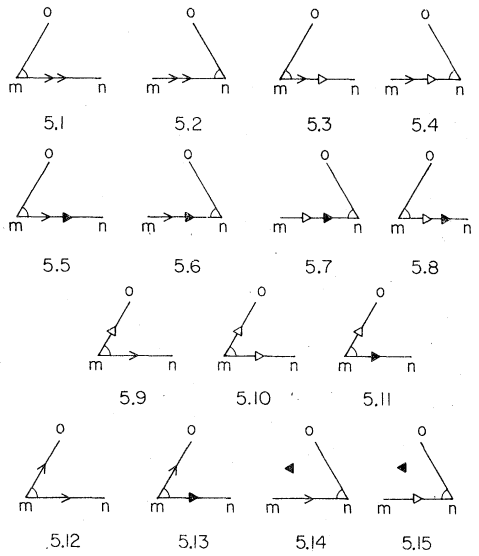

FIG. 5. Illustrations of the kinetic energy terms $T_1 - T_5$.

arrow denotes $(\nabla_i^2 \xi_{ij})$. The sum of diagrams containing 5.1–8 is given by

$$T_1 = \rho^2 \int \tilde{g}_{mn}\tilde{g}_{m0}\tilde{g}_{n0}\left(1+\sum_{\text{cyc}}\chi_{mn0}\right)(\xi r)_{m0}\mu_{mn} \times \cos\theta_m\, d^3r_{mn}\, d^3r_{m0} \tag{4.3}$$

$$\mu = -(\hbar^2/m)[\xi'' r + 4\xi' + 2f'(\xi' r + \xi)/f],$$

while that of diagrams having 5.9–11 is

$$T_2 = \rho^2 \int \tilde{g}_{mn}\tilde{g}_{m0}\tilde{g}_{n0}\left(1+\sum_{\text{cyc}}\chi_{mn0}\right)\xi_{m0}\nu_{mn}\, d^3r_{mn} d^3r_{m0} \tag{4.4}$$

$$\nu = -(\hbar^2/m)(\xi' r + \tfrac{3}{2}\xi + f'\xi r/f).$$

The contribution of terms 5.12, 13 is

$$T_3 = -\frac{\hbar^2}{2m}\rho^2 \int \tilde{g}_{mn}\tilde{g}_{m0}\tilde{g}_{n0}\left(1+\sum_{\text{cyc}}\chi_{mn0}\right)(\xi' r)_{m0} \times \left(\xi' r + \frac{2f'\xi r}{f}\right)_{mn} \cos^2\theta_m\, d^3r_{mn}\, d^3r_{m0}, \tag{4.5}$$

while that of 5.14 and 5.15 is, respectively,

$$T_4 = -\frac{\hbar^2}{m}\rho^2 \int \tilde{g}_{mn}\tilde{g}_{m0}\tilde{g}_{n0}\left(1+\sum_{\text{cyc}}\chi_{mn0}\right)\left(\frac{f'}{f}\right)_{m0} \times (\xi' r)_{mn}(\xi r)_{n0}\cos\theta_m\cos\theta_n\, d^3r_{mn}\, d^3r_{m0}, \tag{4.6}$$

$$T_5 = +\frac{\hbar^2}{m}\rho^2 \int \tilde{g}_{mn}\tilde{g}_{m0}\tilde{g}_{n0}\left(1+\sum_{\text{cyc}}\chi_{mn0}\right)\left(\frac{f'}{f}\right)_{m0} \times \xi_{mn}(\xi r)_{n0}\cos\theta_0\, d^3r_{mn}\, d^3r_{m0}. \tag{4.7}$$

The total $T(=\sum_{i=1,5} T_i)$ is positive and increases rapidly with β (Table I).

The kinetic energy also has terms of type $(\vec{\nabla}_m \sum_{\text{cyc}} \chi_{mn0})\cdot(\vec{\nabla}_m \sum_{\text{cyc}} \chi_{mnp})$, $(\vec{\nabla}_m \sum_{\text{cyc}} \chi_{mn0})\cdot(\vec{\nabla}_m f_{mp})$, and $(\vec{\nabla}_m \sum_{\text{cyc}} \chi_{mn0})\cdot(\vec{\nabla}_m \sum_{\text{cyc}} \chi_{mpq})$. However, it is more consistent to estimate these along with their analogous distribution function diagrams in Sec. V.

The total energy E in this approximation is

$$E = W + U + T, \tag{4.8}$$

and exhibits a minimum with respect to variations in β (Table I) and d (Table II). The $E(d, \beta_{\min})$ is more sensitive to d than $E(d, \beta=0)$,[1] and the $d_{\min}/r_0$ increases from ≈ 1.85 at $0.8\rho_e$ to ≈ 2.05 at $1.2\rho_e$ (Table III). The $E(\rho_{\min})$ is estimated to be -6.72 at $\rho_{\min} = 1.04\rho_e$.

V. CONVERGENCE STUDIES

The "HNC-type" diagrams neglected in Sec. IV can be separated into two groups. Simple examples of group I diagrams are shown in Fig. 6; 6.1–6.3 are distribution-function diagrams that have more than one χ connecting a pair ij; 6.4–6.6 are χ dressings to the kinetic-energy diagrams included in U and T; and 6.7–6.9 are kinetic-energy diagrams not included in U and T. These are diagrams in which there are two or more chains $ij_1k, ij_2k, \ldots, ij_nk$, of type other than C_1, connecting i and k; and their integrand contains the cosines of some of the internal angles of triangles $ij_1k, ij_2k, \ldots, ij_nk$. In contrast, the integrand of a group II diagram has at least one cosine of an internal angle of a triangle ij_1j_2; j_1 and j_2 being particles in two different chains.

Group I diagrams can be easily summed. The χ hypernets in g and the χ dressings of U and T are summed by defining g and $\tilde{g}$ in Eq. (3.3) and (4.2)–(4.7) as

$$g = \tilde{g} = f^2 \exp(C_1 + 2C_2 + 4C_3 + C_4 + 2C_5 + 4C_6 + 2C_7). \tag{5.1}$$

The kinetic-energy diagrams of type 6.7–6.9 are calculated with the help of two functions α_{mn} and γ_{mn} defined as follows:

TABLE III. $E(\rho, d_{\min})$.

ρ/ρ_e	$d_{\min}/r_0$	$E(d_{\min})$
0.8	1.85	−6.22
0.9	1.90	−6.54
1.0	1.95	−6.69
1.1	2.00	−6.68
1.2	2.05	−6.47

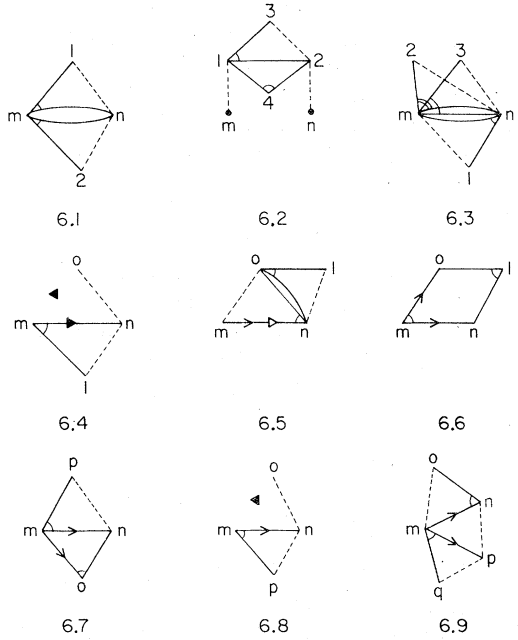

FIG. 6. Examples of "group I" diagrams neglected in Sec. IV.

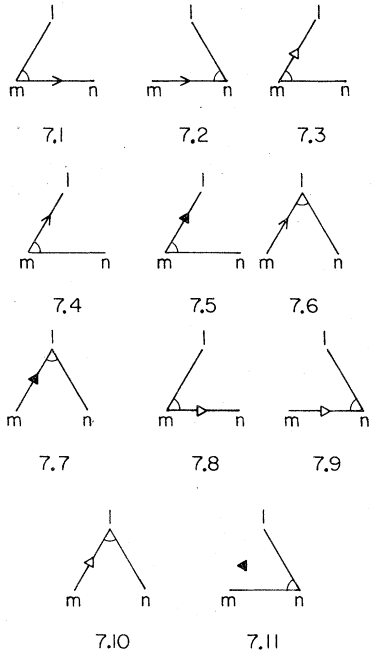

FIG. 7. Diagrammatic illustration of α_{mn} and γ_{mn}.

$$\alpha_{mn}=\rho\int\Phi_{mn1}[2(\xi r)_{m1}(\xi' r)_{mn}\cos\theta_m+\xi_{m1}(\xi r)_{mn}]\,d^3r_1\,, \tag{5.2}$$

$$\begin{aligned}\gamma_{mn}=\rho\int&\left[\Phi_{mn1}\left(\xi' r+\frac{f'\xi r}{f}\right)_{m1}+g_{n1}\left(\frac{gf'\xi r}{f}\right)_{m1}\right]\\&\times[(\xi r)_{mn}\cos^2\theta_m+(\xi r)_{n1}\cos\theta_m\cos\theta_1]\,d^3r_1\\&+\rho\int\Phi_{mn1}[2(\xi r)_{m1}\xi_{mn}\cos\theta_m-\xi_{m1}(\xi r)_{n1}\cos\theta_n]\,d^3r_1\\&+\rho\int\left[\Phi_{mn1}\left(\frac{f'}{f}\right)_{m1}+g_{n1}\left(\frac{gf'}{f}\right)_{m1}\right](\xi r)_{mn}(\xi r)_{n1}\\&\times\cos\theta_m\cos\theta_n\,d^3r_1\,,\end{aligned} \tag{5.3}$$

where

$$\Phi_{mn1}=g_{m1}g_{n1}\left(1+\sum_{\text{cyc}}\chi_{mn1}\right). \tag{5.4}$$

The simplest of the diagrams contributing to α_{mn} (7.1–7.3) and γ_{mn} (7.4–7.11) are shown in Fig. 7. The diagrams of type 6.7 are given by

$$T_6=-\frac{\hbar^2}{2m}\rho\int g_{mn}\,\alpha_{mn}(\alpha_{mn}+2\gamma_{mn})\,d^3r_{mn}\,, \tag{5.5}$$

while those of type 6.8–6.9 are generated by the replacement

$$f'/f\to f'/f+\alpha \tag{5.6}$$

in the Eq. (4.2) for U.

However, the contribution of HNC/4 analogs of group I diagrams, obtained by inserting an additional bond between 1 and 2 in 6.1, 3 and 4 in 6.2, etc., may be comparable to that of the group I diagrams. Consider 6.1 as a typical case; most of the contribution comes from the region in which $r_{mn}\approx r_{m1}\approx r_{m2}\approx\sigma$, where $g\xi r$ (or gf'/f) is peaked. If we sum all chains connecting $n1$ and $n2$ we get $(g-1)_{n1}(g-1)_{n2}$ in the integrand, and the interesting region becomes $\theta_1\approx\theta_2\approx\frac{1}{4}\pi$, where θ_1 and θ_2 are the angles of the triangles $mn1$, $mn2$ at vertex m. Let $\vec{r}_m$ be the origin, $\vec{r}_n$ on the Z axis, $\vec{r}_1$ in the X-Y plane and Φ_2 be the azimuthal angle of $\vec{r}_2$. The Φ_2 integration determines the ratio of 6.1 and its HNC/4 counterpart denoted by 6.1/4. It gives a factor 2π in the contribution of 6.1, and $\sim-\pi$ in that of 6.1/4 if we take $(g-1)_{12}\approx-1$ for $r<\sigma$, 0 for $r>\sigma$. Thus we may expect a reduction of groupI diagrams by a factor of ~2 from their HNC/4 counterparts.

It should be noted that, even though summing diagrams of type 6.1–6.3 by exponentiation of C_{2-7} in Eq. (3.3) may not increase the calculation accuracy significantly, the exponentiation of C_1 does. The contribution of a HNC/4 diagram having two coupled C_1 chains is

$$\frac{\rho^2}{2}\int(g-1)_{m1}(g-1)_{m2}(g-1)_{n1}(g-1)_{n2}(g-1)_{12}\times d^3r_1\,d^3r_2\,, \tag{5.7}$$

and, as we have argued in the case of 6.1, it may well be of order

$$-\frac{1}{4}\left(\rho\int(g-1)_{m1}(g-1)_{n1}\,d^3r_1\right)^2. \tag{5.8}$$

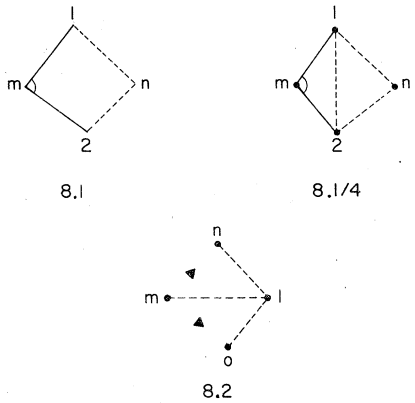

FIG. 8. Examples "group II" diagrams.

However, it is still much smaller than $\frac{1}{2}C_1^2$,

$$\frac{C_1^2}{2}=\frac{1}{2}\left(\rho\int (g-1-C_1)_{m1}(g-1)_{n1}\,d^3r_1\right)^2 \qquad (5.9)$$

because $|C_1| \gg |(g-1)|$, as can be seen from Fig. 4.

A typical group II diagram is shown in Fig. 8.1, its integrand contains $\cos\theta$, where θ is the angle of the triangle $m12$ at vertex m. To estimate the ratio of 8.1 to its HNC/4 counterpart 8.1/4 (Fig. 7) we may express $\cos\theta$ as

$$\cos\theta=\hat{z}_1\hat{z}_2+\hat{x}_1\hat{x}_2\approx\tfrac{1}{2}+\tfrac{1}{2}\cos\phi_2\,. \qquad (5.10)$$

where $\hat{z}_1$, $\hat{z}_2$, $\hat{x}_1$, and $\hat{x}_2$ are projections of unit vectors $\hat{r}_1$ and $\hat{r}_2$, and we have assumed that $\theta_1 \approx \theta_2 \approx \frac{1}{4}\pi$ in the region of interest. Only the $\hat{z}_1\hat{z}_2$ term contributes to 8.1, and thus the ϕ_2 integration gives there a factor π. In 8.1/4 the $\hat{z}_1\hat{z}_2$ term will give $\approx-\frac{1}{2}\pi$, while we may expect ≈-1 from the $\hat{x}_1\hat{x}_2$ term. Thus the ratio

$$\frac{8.1+8.1/4}{8.1}\approx\frac{\pi-\pi/2-1}{\pi}\approx 0.2\,, \qquad (5.11)$$

and in general calculating group II diagrams without their HNC/4 analog will decrease the calculation accuracy. It may be mentioned here that group II diagrams of type 8.2 are summed if the Jackson-Feenberg identity is used to calculate the kinetic energy,[1] and this deteriorates the convergence.[6]

In order to estimate the uncertainty in the calculations discussed in Sec. IV, the diagrams of group I are calculated. At $d=2r_0$ and ρ_e these change the $\beta_{\min}$ significantly from 1.65 to 2.6 but leave the energy unaffected (−6.72 instead of −6.68 in Table I). However, some of the diagrams are quite significant (~0.4 °K), and the small change in E is due to a ~90% cancellation and may not have any significance.

The HNC/4 diagram due to the coupling of two C_1 chains,[1] as well as its correction to the superposition approximation to the three-body distribution function[1] is calculated as follows: Let ζ_{ijk} and $\mathcal{E}_{ij}$ be defined as

$$\zeta_{ijk}=\zeta(\vec{r}_i,\vec{r}_j,\vec{r}_k)$$
$$=\rho\int (g-1)_{i1}(g-1)_{j1}(g-1)_{k1}\,d^3r_1\,, \qquad (5.12)$$

$$\mathcal{E}_{ij}=\frac{\rho}{2}\int \zeta_{ijk}(g-1)_{ik}(g-1)_{jk}\,d^3r_k\,. \qquad (5.13)$$

Multiply the integrands of the equations for C_2–C_7 by $(1+\zeta_{mn1})$, redefine $g,\tilde{g}$ as

$$g=\tilde{g}=f^2\exp(C_1+2C_2+4C_3+C_4+2C_5+4C_6+2C_7+\mathcal{E})\,, \qquad (5.14)$$

multiply integrands of U, T_{1-5} by $(1+\zeta_{mn0})$, and those of α and γ by $(1+\zeta_{mn1})$. This raises the energy at ρ_e, $d=2r_0$, $\beta=2.6$ to −6.61. The g obtained in this calculation has a little more structure. The values at first maxima and minima, respectively, are 1.278 and 0.921 as against 1.266 and 0.942 found for $\beta=1.65$ in the last calculation. From our considerations in Sec. II, and the f' and ηr in Fig. 1 we could have expected a $\beta\approx 2$ at minimum which is in between the 1.65 found in Sec. IV and 2.6 obtained here.

The effect of requiring the two-body $f(r>d)=1$ on the variational energy may be studied by optimizing the Jastrow wave function. The optimum $f-1$ has a $1/r^2$ long-range behavior, and the superposition approximation used in the calculation of U is not valid. Hence, only the results of calculations using the Jackson-Feenberg (JF) identity are available at the HNC and the HNC/4 level. At the HNC level the difference between the energy calculcated with the JF identity at ρ_e with optimum (−4.64 °K) and present (−4.05) f's is large[9]; however, at the HNC/4 level it decreases significantly (−5.24 and −5.05 °K), to ~0.2 °K.[10] The correct energy at ρ_e with the present $f(d=2r_0)$ is −5.67 ± 0.13 °K as known from Monte Carlo calculations or cluster expansions using the $W+U$ form. Thus, one might expect the true effect of optimizing the two-body f to be <0.2 °K.

The energy of liquid ^{4}He may also be influenced by three- (or more-) body forces neglected in Sec. IV. The contribution of the three-body triple dipole interaction[3]

$$v_{td}(\vec{r}_1,\vec{r}_2,\vec{r}_3)=\frac{1500}{(2.556)^9}\frac{1+3(\hat{r}_{12}\cdot\hat{r}_{13})(\hat{r}_{21}\cdot\hat{r}_{23})(\hat{r}_{31}\cdot\hat{r}_{32})}{(r_{12}r_{23}r_{31})^3} \qquad (5.15)$$

is given by

$$W_{td}=\frac{\rho^2}{6}\int g_{mn}g_{m0}g_{n0}\left(1+\sum_{\text{cyc}}\chi_{mn0}\right)^2$$
$$\times(1+\zeta_{mn0})v_{td,mn0}\,d^3r_{mn}\,d^3r_{m0}\,. \qquad (5.16)$$

The W_{td} at ρ_e is found to be +0.15 °K and will significantly compensate the decrease in E by optimizing the f.

VI. CONCLUSIONS

The results of the calculations described in Sec. IV are compared in Fig. 9 with those using (i) only two-body correlations[1] (curve 2B); (ii) optimized two-body correlations plus "perturbative" treatment of three-body correlations[4] (curve 2-op+3-p); (iii) Green's-function Monte Carlo (GFMC) calculation of the hard-sphere model[5] (filled squares); and (iv) GFMC of liquid ^{4}He (filled triangles).[11] The curve (2+3) gives the present results, while the filled circle denotes the experimental equilibrium point.

The effects of long-range correlations and three-body forces are neglected in curves 2B, (2+3), and the filled triangles, while (2-op+3-p) curve and the filled squares take into account the lowering of the energy due to long-range correlations but neglect the roughly equal but opposite effect of three-body forces. Thus the (2-op+3-p) and solid squares should be raised by ≈0.15 °K to make meaningful comparisons. The curves 2B, (2-op+3-p), (2+3) and the squares probably have uncertainties of ≈0.2 °K, while the triangles have lesser uncertainties. The GFMC is in principle "exact"; the uncertainties in its results being due to numerical accuracies and surface effects. The comparison indicates that a good fraction of the difference between the "exact" ground-state energy and the upper bound obtained with two-body correlations can be covered with a rather simple three-body correlation that takes into account the back flows produced by two atoms recoiling from each other in the liquid.

The equilibrium energy and density obtained in (2-op+3-p), (2+3), and GFMC calculations is nearer to experiment than that in the 2B calculation. The inadequacy of the structure of the calculated $g(r)$, and the large value of the equilibrium density are probably because the Lennard-Jones-deBoer-Michels potential has too small a core radius.

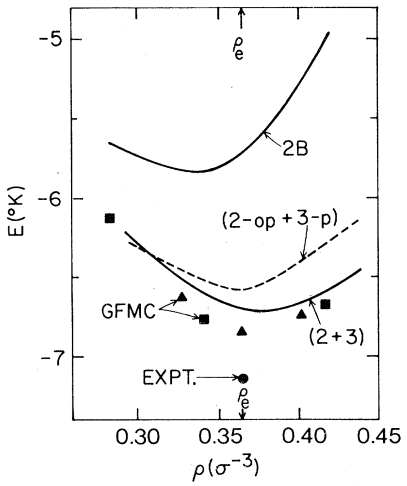

FIG. 9. The $E(\rho)$ of liquid ^{4}He obtained in various calculations.

The required computational effort may more than double if (2.9) is used as a variational wave function instead of its approximation (2.10). However, since (2.9) has only one variational parameter, it may in fact be more economical to use it directly. The present calculations are rather simple and easily extendible to Fermi liquids.

ACKNOWLEDGMENT

This work was supported by NSF PHYS 76-22147.

[1]V. R. Pandharipande and K. E. Schmidt, Phys. Rev. A 15, 2486 (1977).
[2]R. P. Feynman and M. Cohen, Phys. Rev. 102, 1189 (1956).
[3]A. Dalgarno and G. A. Victor, Mol. Phys. 10, 333 (1967).
[4]C. C. Chang and C. E. Campbell, Phys. Rev. B 15, 4238 (1977).
[5]M. H. Kalos, D. Levesque, and L. Verlet, Phys. Rev. A 9, 2178 (1974).
[6]V. R. Pandharipande and H. A. Bethe, Phys. Rev. C 7, 1312 (1973).
[7]V. R. Pandharipande and N. Itoh, Phys. Rev. A 8, 2564 (1973).
[8]R. B. Wiringa and V. R. Pandharipande, Nucl. Phys. A (to be published).
[9]L. J. Lantto, A. D. Jackson, and P. J. Siemens, Phys. Lett. B 68, 311 (1977).
[10]L. J. Lantto (private communication).
[11]M. H. Kalos, Invited talk in the Workshop on Nuclear and Dense Matter, Urbana, Illinois, 1977 (unpublished).